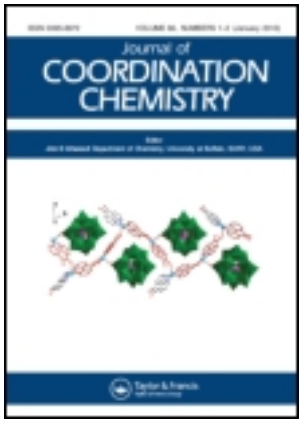

Journal of Coordination Chemistry
Publication details, including instructions for authors and subscription information:
http://www.tandfonline.com/loi/gcoo20

Structures, luminescence, and antibacterial studies of two transition metal complexes involving Schiff bases

De-Yun Ma[ab], Le-Xin Zhang[a], Xuan-Ye Rao[a], Tong-Liang Wu[a], Dong-Hao Li[a], Xiao-Qun Xie[a], Hai-Fu Guo[a] & Liang Qin[a]

[a] School of Chemistry and Chemical Engineering, Zhaoqing University, Zhaoqing, P.R. China

[b] Key Laboratory of Fuel Cell Technology of Guangdong Province, South China University of Technology, Guangzhou, P.R. China

Accepted author version posted online: 07 Aug 2013.Published online: 24 Sep 2013.

To cite this article: De-Yun Ma, Le-Xin Zhang, Xuan-Ye Rao, Tong-Liang Wu, Dong-Hao Li, Xiao-Qun Xie, Hai-Fu Guo & Liang Qin (2013) Structures, luminescence, and antibacterial studies of two transition metal complexes involving Schiff bases, Journal of Coordination Chemistry, 66:18, 3261-3271, DOI: 10.1080/00958972.2013.832230

To link to this article: http://dx.doi.org/10.1080/00958972.2013.832230

Journal of Coordination Chemistry, 2013
Vol. 66, No. 18, 3261–3271, http://dx.doi.org/10.1080/00958972.2013.832230

Structures, luminescence, and antibacterial studies of two transition metal complexes involving Schiff bases

DE-YUN MA*†‡, LE-XIN ZHANG†, XUAN-YE RAO†, TONG-LIANG WU†, DONG-HAO LI†, XIAO-QUN XIE†, HAI-FU GUO† and LIANG QIN*†

†School of Chemistry and Chemical Engineering, Zhaoqing University, Zhaoqing, P.R. China
‡Key Laboratory of Fuel Cell Technology of Guangdong Province, South China University of Technology, Guangzhou, P.R. China

(*Received 16 May 2013; accepted 29 July 2013*)

Two new transition metal complexes of Schiff bases, $[Pd_2(\mathbf{L1})_2Cl_2]$ (**1**) and $[Zn(\mathbf{L2})_2]$ (**2**), [**L1** = N-(4-fluorobenzylidene)-2,6-diisopropylbenzenamine and **L2** = 2,4-dibromo-6-((E)(mesitylimino) methyl)phenol], have been synthesized solvothermally and characterized by elemental analysis, IR-spectroscopy, thermogravimetric analysis, powder X-ray diffraction, UV-vis absorption spectra, and single-crystal X-ray diffraction. Complex **1** is a μ-chloro-bridged dinuclear cyclometallated Pd (II) complex, whereas **2** is mononuclear with the Zn^{II} tetrahedrally coordinated by two **L2**. Both **1** and **2** display photoluminescence in the solid state at 298 K (fluorescence lifetimes $\tau = 22.516$ ns at 468 nm for **1**, $\tau = 3.697$ µs at 490 nm for **2**). These Schiff bases and their metal compounds have been screened for antibacterial activity against several bacteria, and the results are compared with the activity of penicillin.

Keywords: Transition metal complexes; Schiff bases; Luminescence; Antibacterial activity

1. Introduction

Schiff bases are important compounds due to their biological activities [1] and as ligands. Palladium(II) complexes based on Schiff bases have potential applications in luminescence, catalysis, and bacteriostasis [2–4]. However, compared to platinum(II) complexes involving Schiff bases, whose applications as luminescent sensors are of considerable interest in inorganic photochemistry [5, 6], less attention has focused on the luminescent characteristics of palladium(II) complexes [4]. Luminescent cyclopalladated complexes show weak emissions detected only at low temperatures [7] due to the presence of thermally accessible low-lying metal centered states that allow excited states to undergo nonradiative decay [8]. Zn(II) complexes bearing salicylaldiminato ligands have been employed as blue, greenish-white, and red emitters in organic optoelectronics with better stability and efficiency [9–11].

*Corresponding authors. Email: mady@zqu.edu.cn (D.-Y. Ma); liangq@zqu.edu.cn (L. Qin)

In those zinc(II) complexes, the salicylaldiminato ligands are mainly salen with two N and two O donors; reports on luminescent properties of bis(salicylaldiminato) zinc(II) complexes are limited. Many Schiff bases and their metal complexes have been reported to have antimicrobial activities and potential as orally effective iron-chelating agents for treatment of iron overload disease and cancer [12, 13].

Here, we report the synthesis, characterization, luminescence, and antibacterial activities of two new transition metal complexes based on Schiff-base ligands.

2. Experimental

2.1. *Materials and physical measurements*

All chemicals were commercially available and used as received. C, H, and N elemental analyses were carried out using a Vario EL III Elemental Analyzer. Infrared spectra were recorded (4000–400 cm^{-1}) as KBr disks on a Shimadzu IR-440 spectrometer. Thermogravimetric (TG) analyses were performed on an automatic simultaneous thermal analyzer (DTG-60, Shimadzu) under a flow of N_2 at a heating rate of 10 °C/min between ambient temperature and 800 °C. Powder XRD investigations were carried out on a Bruker AXS D8-Advanced diffractometer at 40 kV and 40 mA with Cu-Kα ($\lambda = 1.5406$ Å) radiation. UV-vis absorption spectra were measured using a Shimadzu UV-160A spectrophotometer. Luminescence spectra and lifetimes for crystalline samples were recorded at room temperature on an Edinburgh FLS920 phosphorimeter. Nuclear Magnetic Resonance spectra were recorded on a Bruker Avance 400 MHz spectrometer. ^{1}H-NMR chemical shifts are reported in ppm from tetramethylsilane (TMS) with the solvent resonance as the internal standard ($CDCl_3$, $\delta = 7.26$). ^{13}C-NMR spectra were collected on a 100 MHz spectrometer with complete proton decoupling. Chemical shifts were reported in ppm from TMS with the solvent resonance as internal standard ($CDCl_3$, $\delta = 77.23$). Melting points (uncorrected) were measured with a Mel-Temp apparatus.

2.2. *Solvothermal synthesis*

2.2.1. Preparation of L1. L1 was prepared by condensation of 4-fluorobenzaldehyde (2.48 g, 20 mMol) with 2,6-diisopropylaniline (3.55 g, 20 mMol) in ethanol (20 mL). The solution was refluxed for 4 h and then allowed to cool to room temperature. The yellow precipitate was recrystallized from ethanol to give **L1** as straw yellow crystals. Yield 4.52 g (80%). ^{1}H NMR (400 MHz, $CDCl_3$) δ: 8.15 (s, 1H, C**H**N), 7.10–7.92 (m, 7H, Ar-H), 2.95 [t, $J = 9.16$ Hz, 2H, C**H**$(CH_3)_2$], 1.16 (d, $J = 4.6$ Hz, 12H, CH_3); ^{13}C NMR (100 MHz, $CDCl_3$) δ: 165.7, 164.0, 160.5, 149.0, 137.6, 132.4, 130.6, 130.5, 124.2, 123.1, 116.1, 115.9, 28.0, 23.5; MP: 77–80 °C. Anal. for $C_{19}H_{21}NF$ (%): Calcd C 89.1, H 8.2, N 5.5; Found C 89.5, H 7.9, N 5.3. FT-IR (KBr, cm^{-1}): 3465(s), 2964(m), 1647(s), 1599(s), 1508 (s), 1464(w), 1442(w), 1385(w), 1363(w), 1294(m), 1226(m), 1176(m), 1153(m), 1093(w), 1058(w), 933(w), 877(w), 837 (m), 800(w), 784(w), 748(s), 688(w), 595(w), 561(w), 511 (w), 486(w).

2.2.2. Preparation of L2. L2 was prepared by the same procedure as for **L1** except that 4-fluorobenzaldehyde and 2,6-diisopropylaniline were replaced by 3,5-dibromosalicylaldehyde

and 2,4,6-trimethylaniline. Yield 6.213 g (78%). ^{1}H NMR (400 MHz, $CDCl_3$) δ: 14.33 (s, 1H, OH), 8.22 (s, 1H, C**H**N), 7.25–7.76 (m, 4H, Ar-H), 2.23 (d, $J = 51.6$ Hz, 9H, CH_3); ^{13}C NMR (100 MHz, $CDCl_3$) δ: 164.8, 157.7, 144.2, 138.2, 135.4, 133.3, 129.3, 128.4, 120.3, 112.3, 110.1, 20.8, 18.5; MP: 89–93 °C. Anal. for $C_{16}H_{14}Br_2NO$ (%): Calcd C 48.5, H 3.5, N 3.5; Found C 48.9, H 3.2 N 3.1. FT-IR (KBr, cm^{-1}): 3460(s), 2920(m), 1624(s), 1562(w), 1493(m), 1447(m), 1378(w), 1291(w), 1221(w), 1195(w), 1157(w), 1122(m), 1038(m), 874 (m), 847(m), 763(w), 724(w), 686 (s), 552(w), 487(w).

2.2.3. Preparation of $[Pd_2(L1)_2Cl_2]$ (1). Na_2PdCl_4 (0.0887 g, 0.5 mMol) was dissolved in methanol (10 mL). **L1** (0.256 g, 1 mMol) was added and the mixture stirred at room temperature for 5 h under an anhydrous atmosphere. The resulting mixture was filtered under reduced pressure. The collected solid was washed with diethyl ether and dried in air to give yellow crystals that were purified by recrystallization from methylene chloride (15 mL) and hexane (10 mL). Yield 0.175 g (82%). Anal. for $C_{38}H_{42}N_2Cl_2F_2Pd_2$ (%): Calcd C 53.8, H 5.0, N 3.3; Found C 53.5, H 5.2, N 3.5. FT-IR (KBr, cm^{-1}): 3458(s), 2960(m), 1627(vs), 1580(s), 1508(vs), 1462(s), 1450(m), 1384(w), 1361(w), 1327(w), 1298(w), 1253(w), 1220 (w), 1178(w), 1112(m), 1058(w), 1032(w), 929(w), 918(w), 877(m), 815(m), 797(m), 754 (s), 703(w), 669(w), 577(w), 505(w) 482(w), 435(w), 413(w).

2.2.4. Preparation of $[Zn(L2)_2]$ (2). Complex **2** was prepared by the same procedure as **1** except that **L1** was replaced with **L2**. Yield 0.12 g (86%). Anal. for $C_{32}H_{28}N_2O_2Br_4Zn$ (%): Calcd C 44.8, H 3.3, N 3.3; Found C 45.3, H 3.2, N 3.0. FT-IR (KBr, cm^{-1}): 3465(s), 2975 (m), 2916(s), 1614(vs), 1473(s), 1440(s), 1309(m), 1199(m), 1120(w), 1016(w), 997(w), 960(w), 945(w), 844(m), 756(s), 694(s), 623(w), 590(w), 555(m), 498(s), 476(m), 424(w), 401(s).

2.3. *Antibacterial activity tests*

In vitro bacterial activities of the Schiff bases and their metal complexes were tested using the paper disk diffusion method. The chosen strains were G(+) *Staphylococcus aureus*, *Bacillus cereus* , *Rhizopus,* and *Escherichia coli*. The liquid medium containing the bacterial subcultures was autoclaved for 20 min at 15 lb pressure before inoculation. The bacteria were cultured for 24 h at 35 °C in an incubator. Mueller Hinton broth was used for preparing basal media for the bioassay of the organisms. Nutrient agar was poured onto a Petri plate and allowed to solidify. The test compounds were dissolved in DMF and added dropwise to 10 mm diameter paper disks placed in the center of the agar plates. The plates were then kept at 5 °C for 1 h and transferred to an incubator maintained at 35 °C. The width of the growth inhibition zone around the disk was measured after 24 h of incubation. Four replicates were taken for each treatment. In order to clarify any participating role of DMF in the biological screening, separate control studies were carried out with the solutions of DMF alone and they showed no activity against any bacterial strains.

2.4. *X-ray crystallography*

Single crystal X-ray diffraction analyses of **1** and **2** were performed on a Bruker Apex II CCD diffractometer operating at 50 kV and 30 mA using Mo-Kα radiation ($\lambda = 0.71073$ Å).

Data collection and reduction were performed using APEX II software [14]. Multiscan absorption corrections were applied for all the data-sets using SADABS, as included in the APEX II program [14]. Small residual absorption effects were treated with XABS2 [15]. The structure was solved by direct methods and refined by least squares on F^2 using the SHELXTL program package [16]. All nonhydrogen atoms were refined with anisotropic displacement parameters. Hydrogens attached to carbon and oxygen were placed in geometrically idealized positions and refined using a riding model. Crystallographic data are listed in table 1. Selected bond lengths and angles and H-bonding parameters for the compounds are given in tables 2 and 3, respectively.

Table 1. Crystal and refinement data of **1** and **2**.

Compounds	**1**	**2**
Empirical formula	$C_{38}H_{42}N_2Cl_2F_2Pd_2$	$C_{32}H_{28}Br_4N_2O_2Zn$
Formula weight	848.44	857.57
Temperature (K)	296(2)	296(2)
Crystal system	Monoclinic	Monoclinic
Space group	$P2_1/c$	$P2_1/n$
a (Å)	11.2951(12)	9.681(2)
b (Å)	10.3255(11)	16.668(3)
c (Å)	16.9093(17)	20.048(4)
β (°)	105.552(2)	100.629(4)
V (Å^3)	1899.9(3)	3179.5(11)
Z, D (Mg.m^3)	2, 1.483	4, 1.792
Limiting indices	$-13 \le h \le 11$, $-12 \le k \le 12$, $-20 \le l \le 19$	$-11 \le h \le 11$, $-19 \le k \le 18$, $-24 \le l \le 22$
Reflections collected/unique	10,171/3399	17,682/5716
$F(000)$	856	1680
θ (°)	2.72–25.20	2.07–25.20
Goodness of fit on F^2	1.085	1.015
$R(I>2\sigma)$	$R_1 = 0.0286$ $wR_2 = 0.0903$	$R_1 = 0.0461$ $wR_2 = 0.1147$
R (all data)	$R_1 = 0.0411$ $wR_2 = 0.1178$	$R_1 = 0.0820$ $wR_2 = 0.1322$
Largest diff. peak and hole (Å^{-3})	0.99, −1.25	0.569 and −0.873

$R = \sum(||F_o| - |F_c||)/\sum|F_o|$.
$wR = [\sum w(F_o^2 - F_c^2)^2/\sum w(F_o)^2]^{1/2}$.

Table 2. Selected bond lengths and angles of **1** and **2**.

1			
Pd1–N1	2.027(3)	Pd1–C15	1.962(3)
Pd1–Cl1	2.3226(9)	Pd1–Cl1^{i}	2.4433(9)
C15–Pd1–N1	81.57(13)	C15–Pd1–Cl1	94.52(11)
N1–Pd1–Cl1	176.09(8)	C15–Pd1–C11^{i}	174.82(11)
N1–Pd1–Cl1^{i}	96.77(9)	Cl1–Pd1–Cl1^{i}	87.14(3)
2			
Zn1–N1	2.007(4)	Zn1–N2	2.000(4)
Zn1–O1	1.926(4)	Zn1–O2	1.924(3)
O2–Zn1–O1	111.27(17)	O2–Zn1–N2	95.70(16)
O1–Zn1–N2	110.52(17)	O2–Zn1–N1	115.18(17)
O1–Zn1–N1	95.85(16)	N1–Zn1–N2	128.57(18)

Symmetry codes: (i) $1-x$, $1-y$, $-z$.

Table 3. Hydrogen bond geometries for **1** and **2** (Å, °).

D–H···A	*d*(D–H)	*d*(H···A)	*d*(D···A)	∠D–H···A
1				
C7–H7···N1	0.98	2.46	2.884(9)	106
C9–H9B···F1^{ii}	0.96	2.52	3.359(4)	145
C10–H10···N1	0.98	2.40	2.887(8)	110
C16–H16···Cl1	0.93	2.72	3.255(5)	118
2				
C14–H14B···O2	0.96	2.39	3.330(1)	166
C32–H32C···O1	0.96	2.52	3.446(8)	163

Symmetry codes: (ii) $1-x$, $0.5+y$, $0.5-z$.

3. Results and discussion

3.1. *Structure of 1*

To prepare **1**, the Schiff base was treated with Na_2PdCl_4 in equimolar amounts at room temperature in methanol. The reactions proceeded without reflux under mild conditions, thus preventing oxidation of Pd(II) to Pd(IV) [14].

The molecular structure of **1** is shown in figure 1(a). Selected bond distances and angles are given in table 2. In **1**, each **L1** is bonded to the di-μ-chloro-bridged unit through nitrogen and an aromatic carbon, providing two equivalent five-membered N–C–Pd–C-chelate rings. The geometry at Pd(II) in **1** is square planar (∠ N1–Pd1–Cl1 = 96.77(9)°, ∠ Cl1–Pd1–Cl1 = 87.14(3)°, symmetry code: i = $1-x$, $1-y$, $-z$) with the two cyclometallated ligands in a *trans* arrangement with respect to the Pd···Pd axis. The Pd1–C15 bond [1.963 (2) Å] is shorter than the expected value of 2.08 Å based on the sum of the covalent radii of carbon and palladium, but consistent with those found for related complexes where partial multiple-bond character of Pd–C was assumed [17, 18]. The Pd1–N1 bond distance (2.027(3) Å) is in agreement with the sum of covalent radii for nitrogen and palladium [19], and similar to values reported previously [17, 18]. The lengths of the Pd–Cl bonds *trans* to C (2.443(2) Å) and the Pd–Cl bonds *trans* to N (2.323(4) Å) reflect the different *trans* influences exerted by the phenyl carbon and nitrogen. In the five-membered chelate rings, Pd1, N1, C13, C14 and C15 are essentially planar. The bite angle [C15–Pd1–N1 = 81.55(4)°] is in agreement with those found in a structurally related μ-Cl dimer [18]. In the crystal of **1**, an infinite chain is formed through C9–H9B···F1 hydrogen bonding interactions (figure 1(b)). Moreover, intramolecular C–H···N and C–H···Cl hydrogen bonds are also observed (table 3).

3.2. *Structure of 2*

Single-crystal X-ray diffraction analysis revealed that **2** adopts a distorted tetrahedral geometry with Zn^{II} chelated by two bidentate **L2** *via* the phenolate oxygen and imine nitrogen (figure (2a)). The O-Zn-O angle in **2** (111.27(17)°) is close to values (105–112.5°) in similar bis-salicylaldiminato zinc complexes ($NR^2C_7H_{5-x}(R^1)_xO)_2Zn$ [x = 1 or 2; R^1 = Me, ^{t}Bu, Cl, OMe; R^2 = 2,6-^{i}Pr$_2$C$_6$H$_3$] [20], while the N–Zn–N angle in **2** (128.57(18)°) is also close to those in the latter complexes (122.9–128.9°). The two dihedral angles between the 2,4,6-trimethylphenyl ring and the six-membered chelating ring are 75.29 and 87.97°, respectively. The two six-membered chelating rings are nearly planar with zinc lying 0.041 and 0.052 Å out of the plane, and they are closely perpendicular to each other with the dihedral angle of 86.78°. The imino C = N bonds in **2** retain their double-bond character at 1.288(6) and

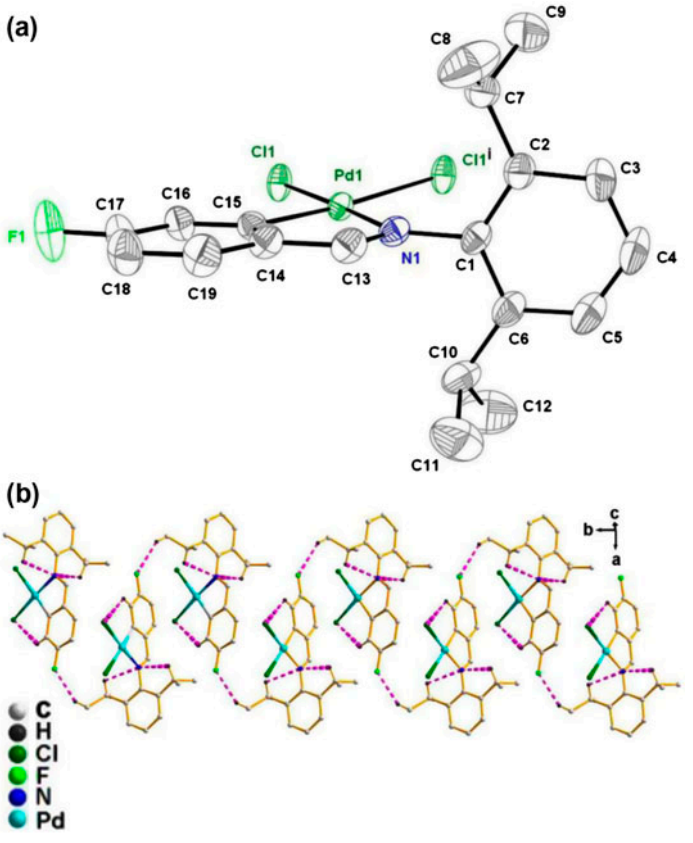

Figure 1. (a) The molecular structure of **1** with numbering scheme (30% probability ellipsoids). All hydrogens are omitted for clarity. Symmetry code: (i) 1−*x*, 1−*y*, −*z*; (b) view of an infinite chain of **1** formed by C9–H9B···F1 hydrogen bonding interactions with *pink dashes*. (see http://dx.doi.org/10.1080/00958972.2013.832230 for color version.)

1.292(6) Å. Mononuclear molecules are connected into a 1-D infinite chain through intermolecular $\pi\cdots\pi$ stacking interactions between benzene rings (Cg1 and Cg2) of **L2** with a centroid-to-centroid distance of 3.717(4) Å (figure 2(b)) (Cg1 and Cg2 are the centroids of C1–C6 and C17–C22 rings, respectively). Weak intramolecular C–H···O hydrogen bonds are also observed (table 3).

3.3. *Powder X-ray diffraction analysis*

In order to check the purity of **1** and **2**, bulk samples were measured by X-ray powder diffraction at room temperature. As shown in figure S1, the peak positions of the experimental patterns are in agreement with the simulated patterns, indicating purity of the complexes.

3.4. *Infrared spectra*

FT-IR spectra of **L1**, **L2**, **1,** and **2** were recorded as KBr pellets (figure S2). In the IR spectrum, moderate bands at 2964 cm^{-1} for **L1**, 2920 cm^{-1} for **L2**, 2960 cm^{-1} for **1,** and 2916

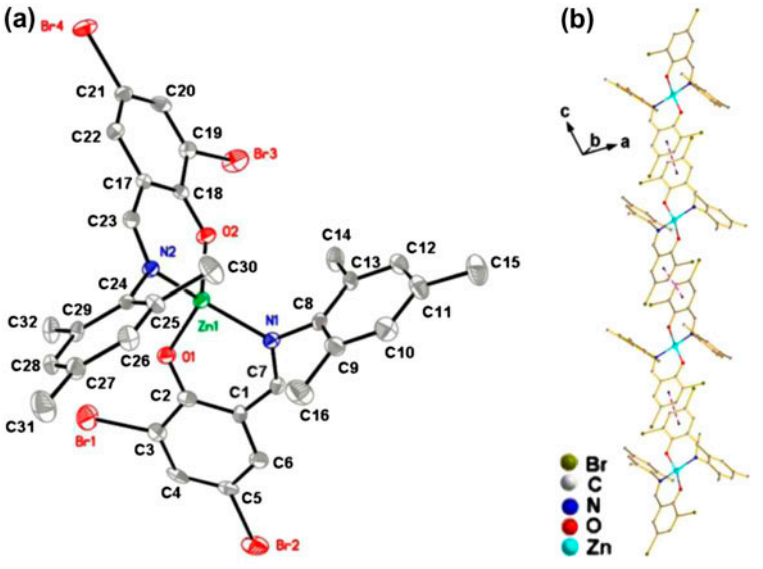

Figure 2. (a) The molecular structure of **2** with numbering scheme (30% probability ellipsoids). All hydrogens are omitted for clarity; (b) view of an infinite chain of **2** formed by intermolecular $\pi\cdots\pi$ stacking interactions with *pink dashes*. (see http://dx.doi.org/10.1080/00958972.2013.832230 for color version.)

Table 4. Photophysical data of ligands and complexes.

Compounds	Medium (T/K)	λ/nm (e/dm^3 mol^{-1} cm^{-1})	Emission λ/nm
L1	DMF (298)	253 (32,800), 315 (12,700)	Non-tested
1	DMF (298)	271 (34,000), 371 (11,500)	Non-tested
L2	DMF (298)	254 (30,140), 286 (28,800), 349 (11,520)	Non-tested
2	DMF (298)	267 (33,320), 317 (13,420), 381 (14,400)	Non-tested
1	Solid (298)	Non-tested	468, 542, 610, 687, 713, 765
2	Solid (298)	Non-tested	490

cm^{-1} for **2** are associated with the methyl (–CH_3) or methylene (–CH_2–) stretches. The features at 1647 cm^{-1} for **L1**, 1624 cm^{-1} for **L2**, 1627 cm^{-1} for **1,** and 1614 cm^{-1} for **2** may be assigned to –CH = N– stretch. Absorptions of –CH = N– in **1** and **2** are clearly blue-shifted against the related ligands, perhaps due to the conjugative effect between metal ions and ligands.

3.5. *Thermogravimetric analysis of 1 and 2*

TG and differential thermal analysis (DTA) curves of **1** and **2** are shown in figure S3. Both structures show good thermal stability as no clean weight-loss step occurs below 533 K for **1** and 613 K for **2**. The DTA trace of **2** shows superior endotherm to **1**, indicating that **2** has better thermal stability than **1**. Weight losses above 533 K and 613 K correspond to decomposition of the framework structures.

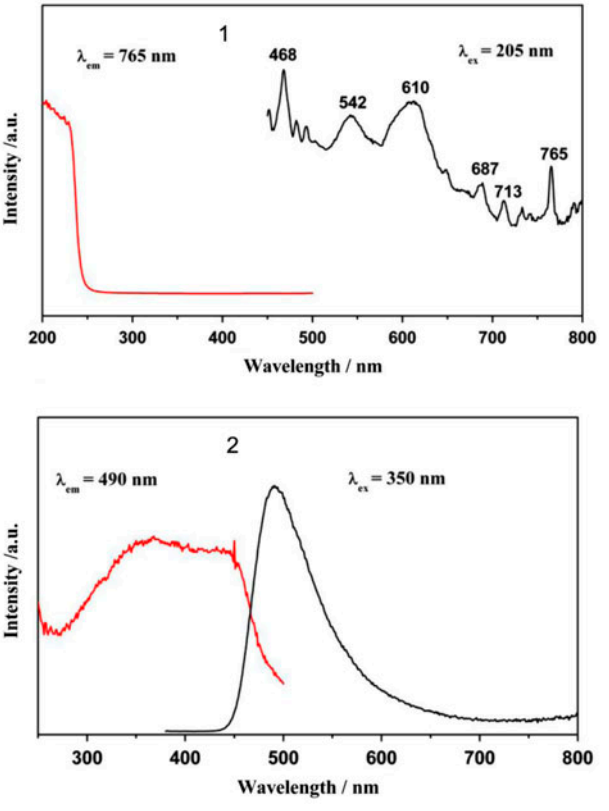

Figure 3. Solid-state excitation and emission spectra of **1** and **2** at room temperature.

3.6. *Electronic absorption and emission properties*

Photophysical data for **L1**, **L2**, **1,** and **2** are summarized in table 4. **L1**, **L2**, **1**, and **2** show low-energy absorptions at *ca.* 300–400 nm and higher energy bands at *ca.* 250–300 nm in DMF (figure S4). From 200–400 nm, the B bands of **L1** and **L2** attributed to π-π* transition are observed at 253 nm for **L1** and 254, 286 nm for **L2**. The absorptions at 315 nm for **L1** and 349 nm for **L2** correspond to the K band of the charge transition between benzene and –C = N–. The high energy absorptions are assigned as intraligand (IL) transitions of **1** and **2** based on their similarity to that of **L1** (253 nm) and **L2** (254 and 286 nm). With reference to previous spectroscopic work on a series of *cis*- and *trans*-[$M(PR_3)_2(X)(Y)$] (M = Pd, Pt) [21–23], [$Ni(PMe_3)_3X_2$] [24], [$Pd_2(P\hat{}P)_2X_4$] [25], [Pd(dbcpe)X_2] [26], [Ar^1 N = $HCAr^2$-$O]_2Zn$ [27], and the close analogy of palladium(II) compounds with the platinum analogs and the nickel(II) congeners, the low energy absorption at ca. 350–400 nm is tentatively assigned as a ligand-to-metal charge transfer transition in **1** and **2**. Electronic absorption spectra of the complexes in the maximum absorption wavelength are red-shifted relative to the ligands due to perturbation of the intraligand π-π* transition of the ligands by metal.

As part of a continuing program dedicated to luminescent systems, the spectroscopic behavior of **1** and **2** are presented. The solid-state emission luminescence spectrum of **1** at room temperature upon excitation at 205 nm is shown in figure 3. The spectrum shows sev-

eral bands at $\lambda_{max} = 468$, 542, 610, 687, 713, and 765 nm, respectively. Both the absorption and solid-state excitation spectra for **1** reveal the presence of low-energy ligand field states in the 300–400 nm spectral region. The high-energy structured band of **1** is assigned to a transition to a ^{3}IL excited state [4]. Complex **2** emits strong blue light in the solid state at room temperature with maximal emission wavelength at 490 nm (excitation wavelength 350 nm, figure 3).

Zinc plays a dual role in luminescence of **2** as pointed out in the literature for coordination complexes [28]. First, the formation of covalent bonds between Zn and O *via* π-donation of lone-pair electrons on O to Zn changes the emission energy due to the lowering of the energy gap between π^* and π. Second, the coordination of the ligands with Zn increases the rigidity of the ligands, which can diminish the loss of energy *via* vibrational motion and increase the emission efficiency. The emission maximum of **L2** is blue-shifted compared to the free ligand (figure S5) in the solid state, due to the disappearance of the intramolecular hydrogen bonding in **L1** after coordination with zinc [26]. The luminescent lifetimes of **1** and **2** using an Edinburgh FLS S920 phosphorimeter with a 450 W xenon lamp as excitation source are for **1** $\tau = 22.516$ ns at 468 nm and for **2** $\tau = 3.697$ µs at 490 nm (figure 4). Complex **2** possesses a longer fluorescence lifetime than other zinc complexes involving Schiff bases [29], and so could be used for light-emitting luminescent materials.

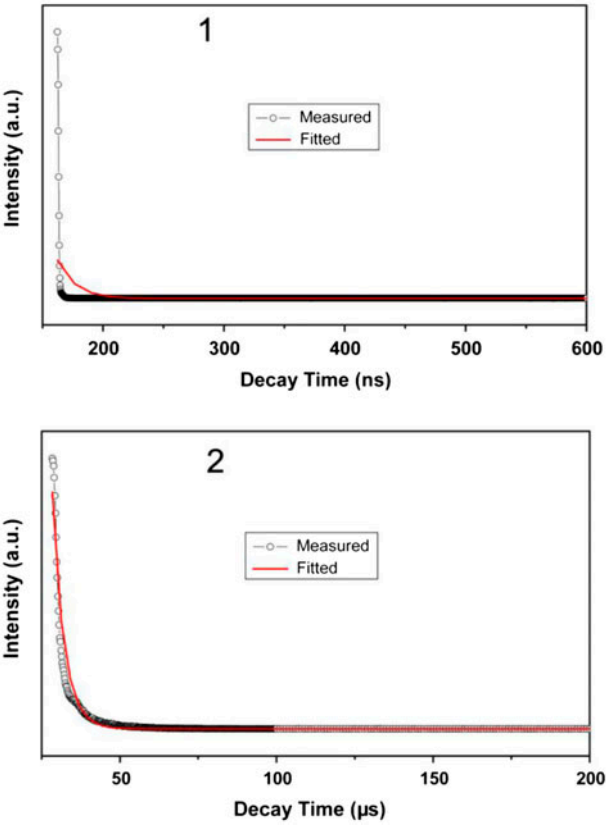

Figure 4. Luminescent lifetimes for **1** and **2** in the solid state at room temperature.

Table 5. Antibacterial activities of ligands and complexes.

Entry	g/disk	Zone of inhibition (mm)			
		S. aureus	*B. cereus*	*Rhizopus*	*E. coli*
L1	20	23	19	0	24
	10	14	8	0	10
	2	0	0	0	0
1	20	27	24	0	26
	10	17	13	0	15
	2	5	0	0	7
L2	20	25	21	0	26
	10	11	8	0	13
	2	0	0	0	0
2	20	28	25	0	24
	10	15	13	0	10
	2	6	0	0	9
Penicillin	20	34	12	0	0
	10	14	0	0	0
	2	0	0	0	0
DMF	20	–	–	–	
	10	–	–	–	–
	2	–	–	–	–

3.7. *Biological activity tests*

Transition metal-based complexes involving N-containing ligands have gained increasing recognition due to their potential application in bacteriostasis [30–33]. The susceptibility of certain strains of bacterium towards **L1**, **L2**, **1,** and **2** were judged by measuring the size of their bactericidal diameters (*vide supra*). The results are given in table 5. The effect against *S. Aureus* were close to that of sodium penicillinate. All of the ligands and complexes showed inhibition diameters larger than sodium penicillinate against *B. cereus*. Compared to **L1**, **L2**, **1,** and **2,** which show good activities, penicillin is ineffective against *E. coli*. However, similar to sodium penicillinate, the four tested samples showed no appreciable activity. The complexes were more effective than ligands. It is possible that the ligand may be activated by the metal ion [34]. El-Sherif reported a series of palladium complexes that show antibacterial activities against *S. pyogenes* and *E.coli* bacteria at 1, 2.5, and 5 mg/mL in DMSO in which the activities were smaller in the complexes than in ligands [35]. Also, the results obtained for **1** and **L** show better antibacterial activities compared to platinum(II) and palladium(II) complexes based on Schiff bases [36].

4. Conclusion

We have described synthesis and characterization of two new transition metal complexes based on Schiff-base ligands. Both **1** and **2** show good thermal stability and exhibit photoluminescence in the solid state at room temperature (τ = 22.516 ns at 468 nm for **1**, τ = 3.697 μs at 490 nm for **2**), suggesting utility as light-emitting luminescent materials. The antibacterial activity tests showed that the ligands and complexes exhibited superior biological activity against *S. aureus*, *B. cereus,* and *E. coli*.

Supplementary material

Figure S1 shows the experimental and simulated XRPD patterns of **1** and **2**. Figure S2 shows the FT-IR spectra of the ligands and complexes. Figure S3 shows the TG and DTA curves of

1 and **2**. Figure S4 shows the UV-visible absorption spectra of the ligands and complexes in DMF. Figure S5 shows the excitation and emission spectra of **L2**. The cif files for **1** and **2** have been deposited with the Cambridge Crystallographic Data Center. CCDC Nos. 907217 and 937161 contain the supplementary crystallographic data for this paper. Copies of the data can be obtained free of charge from the Director, CCDC, 12 Union Road, Cambridge CB2 1EZ, UK (Fax: +44-1223-336-033; E-mail: deposit@ccdc.cam.ac.uk).

Acknowledgments

This work was partially supported by Zhaoqing University Undergraduates Innovating Experimentation Project, Research Fund of Key Laboratory of Fuel Cell Technology of Guangdong Province, Foundation for Distinguished Young Talents in Higher Education of Guangdong Province (2012LYM_0134), Science and Technology Planning Project of Zhaoqing City (2012G013), and Zhaoqing University with doctoral start-up funds.

References

[1] S. Kumar, M.S. Niranjan, K.C. Chaluvaraju, C.M. Jamakhandi, D.J. Kadadevar. *J. Curr. Pharm. Res.*, **01**, 39 (2010).
[2] V.K. Jain, L. Jain. *Coord. Chem. Rev.*, **249**, 3075 (2005).
[3] J.R. Anacona, E. Bastardo. *Transition Met. Chem.*, **24**, 478 (2005).
[4] S.W. Lai, T.C. Cheung, M.C.W. Chan, K.K. Cheung, S.M. Peng, C.M. Che. *Inorg. Chem.*, **39**, 255 (2000).
[5] S.D. Cummings, R. Eisenberg. *J. Am. Chem. Soc.*, **118**, 1949 (1996).
[6] K.H. Wong, M.C.W. Chan, C.M. Che. *Chem. Eur. J.*, **5**, 2845 (1999).
[7] F. Neve, A. Crispini, C. DiPietro, S. Campagna. *Organometallics*, **21**, 3511 (2002).
[8] G.R. Crosby. *Acc. Chem. Res.*, **8**, 231 (1975).
[9] K.H. Chang, C.C. Huang, Y.H. Liu, Y.H. Hu, P.T. Chou, Y.C. Lin. *J. Chem. Soc., Dalton Trans.*, 1731 (2004)
[10] P.F. Wang, Z.R. Hong, Z.Y. Xie, S.W. Tong, O.Y. Wong, C.S. Lee, N.B. Wong, L.S. Huang, S.T. Lee. *Chem. Commun.*, 1664 (2003).
[11] A.C.W. Leung, J.H. Chong, B.O. Patrick, M.J. MacLachlan. *Macromolecules*, **36**, 5051 (2003).
[12] D.Y. Ma, L.X. Zhang, X.Y. Rao, T.L. Wu, D.H. Li, X.Q. Xie. *J. Coord. Chem.*, **66**, 1486 (2013).
[13] E.W. Yemeli Tido, G.O.R. Alberda van Ekenstein, A. Meetsma, P.J. Van Koningsbruggen. *Inorg. Chem.*, **47**, 143 (2007).
[14] Bruker. *APEXII software,* (*Version 6.3.1*), Bruker AXS Inc., Madison, Wisconsin, USA (2004).
[15] S. Parkin, B. Moezzi, H. Hope. *J. Appl. Crystallogr.*, **28**, 53 (1995).
[16] G.M. Sheldrick. *Acta Crystallogr.*, **A64**, 112 (2008).
[17] Y. Fuchita, K. Yoshinaga, T. Hanaki, H. Kawano, J. Kinoshita-Nagaoka. *J. Organomet. Chem.*, **580**, 273 (1999).
[18] A. Crispini, G.D. Munno, M. Ghedini, F. Neve. *J. Organomet. Chem.*, **427**, 409 (1999).
[19] L. Pauling. *The Nature of Chemical Bond*, Cornell University Press, New York (1960).
[20] D.J. Darensbourg, P. Rainey, J. Yarbrough. *Inorg. Chem.*, **40**, 986 (2001).
[21] C.K. Jørgensen. *Prog. Inorg. Chem.*, **18**, 577 (1970).
[22] A.B.P. Lever. *Inorganic Electronic Spectroscopy*, 2nd Edn, Elsevier, Amsterdam (1984).
[23] D.A. Roberts, W.R. Mason, G.L. Geoffroy. *Inorg. Chem.*, **20**, 789 (1981).
[24] J.M. Dawson, T.J. McLennan, W. Robinson, A. Merle, M. Dartiguenave, Y. Dartiguenave, H.B. Gray. *J. Am. Chem. Soc.*, **96**, 4428 (1074).
[25] C.B. Pamplin, S.J. Rettig, B.O. Patrick, B.R. James. *Inorg. Chem.*, **42**, 4117 (2003).
[26] X.X. Lu, E.C.C. Cheng, N. Zhu, V.W.W. Yam. *Dalton Trans.*, 1803 (2006)
[27] Q. Su, Q.L. Wu, G.H. Li, X.M. Liu, Y. Mu. *Polyhedron*, **26**, 5053 (2006).
[28] N.I. Nijegorodov, W.S. Downey. *J. Phys. Chem.*, **98**, 5639 (1994).
[29] Y.P. Tong, S.L. Zheng, X.M. Chen. *Eur. J. Inorg. Chem.*, **2005**, 3734 (2005).
[30] M.N. Patel, P.A. Dosi, B.S. Bhatt. *J. Coord. Chem.*, **65**, 3833 (2012).
[31] L. Ma, J. Zhang, F. Zhang, C. Chen, L. Li, S. Wang, S. Li. *J. Coord. Chem.*, **65**, 3160 (2012).
[32] B. Roopashree, V. Gayathri, H. Mukund. *J. Coord. Chem.*, **65**, 1354 (2012).
[33] N.T. Abdel-Ghani, A.M. Mansour. *J. Coord. Chem.*, **65**, 763 (2012).
[34] O.E. Offiong, E. Nfor, A.A. Avi. *Transition Met. Chem.*, **25**, 369 (2000).
[35] A.A. El-Sherif. *J. Coord. Chem.*, **64**, 2035 (2011).
[36] M.K. Biyala, K. Sharma, M. Swami, N. Fahmi, R.V. Singh. *Transition Met. Chem.*, **33**, 377 (2008).